Dominant Patterns of Climate Variability in the Atlantic Ocean during the Last 136 Years*

YVES M. TOURRE, BALAJI RAJAGOPALAN, AND YOCHANAN KUSHNIR

Lamont-Doherty Earth Observatory, Columbia University, Palisades, New York

(Manuscript received 15 July 1997, in final form 27 July 1998)

ABSTRACT

Dominant spatiotemporal patterns of joint sea surface temperature (SST) and sea level pressure (SLP) variability in the Atlantic Ocean are identified using a multivariate frequency domain analysis. Five significant frequency bands are isolated ranging from the quasi biennial to the quasi decadal. Two quasi-biennial bands are centered around 2.2- and 2.7-yr periods; two interannual bands are centered around 3.5- and 4.4-yr periods; the fifth band at the quasi-decadal frequency is centered around 11.4-yr period. Between 1920 and 1955, the quasi-decadal band is less prominent compared to the quasi-biennial bands. This happens to be the period when SLP gradually increased over the Greenland–Iceland regions. The spatial pattern at the quasi-decadal frequency displays an out-of-phase relationship in the SLP in the vicinity of the subtropical anticyclones in both hemispheres (indicative of an out-of-phase quasi-decadal variability in the North and South Atlantic Hadley circulation). The quasi-decadal frequency also displays an out-of-phase relationship in the SSTs north and south of the mean position of the intertropical convergence zone (ITCZ). This short-lived structure, lasting for approximately two years, supports the argument that a tropical SST dipole pattern is one of the characteristics of the quasi-decadal signal. All five frequency bands represent to some extent fluctuations of the North Atlantic oscillation and are associated with tropical Atlantic Ocean warming (cooling) with different spatial evolution. The two interannual bands show opposite SST evolution to the south of the ITCZ, that is, southeastward evolution from the western tropical Atlantic for the 3.5-yr period and westward spreading from the eastern tropical Atlantic for the 4.4-yr period. Moreover, a significant coherence (with a 1-yr phase lag) is found between the SST time series along the equatorial Atlantic obtained from the 3.5-yr period, and the SST time series in the Niño3 area in the Pacific. It is cautiously argued that the 3.5-yr period is largely associated with the global El Niño–Southern Oscillation phenomenon, while the evolution of the 4.4-yr period depends more upon Atlantic local conditions.

1. Introduction

In the Pacific Ocean, where the El Niño–Southern Oscillation (ENSO) phenomenon dominates the interannual variability, there is a generally understood scenario of coupled ocean–atmosphere tropical processes (Cane and Zebiak 1985). Consequently, understanding and predicting the Pacific El Niño phenomenon have considerably improved in the last 10 years (Cane et al. 1986; Barnett et al. 1988; Neelin et al. 1994; Chen et al. 1995). The relationship between sea surface temperature (SST) and sea level pressure (SLP) is well documented (e.g., Rasmusson and Arkin 1985) and since then distinctions have been made between the global ENSO signal (Kawamura 1994; Lanzante 1996; Tourre and White 1995), the decadal climate variability (Latif and Barnett 1994), and the "ENSO-like decade-to-century variability" (Zhang et al. 1996). The Atlantic climate variability, on the other hand, is characterized by a strong basin-wide and broad-banded coherence between ocean and atmosphere anomalies. For example, in the equatorial Atlantic "conditions at times (1963, 1973, or 1984) resemble El Niño" (Merle 1980; Philander 1990) and a "significant part of observed variability can be described by an equatorial mode akin to ENSO" (Zebiak 1993). In the North Atlantic, surface atmospheric circulation is dominated by the semi-permanent Icelandic low and Azores high. The interannual fluctuations of these two cells are anticorrelated and contribute to the North Atlantic oscillation (NAO). The NAO displays quasi-biennial, quasi-decadal, and multidecadal variability (Hurrell 1995). Quasi-decadal to interdecadal variability has been identified in the Atlantic ocean–atmosphere system as well (Deser and Blackmon 1993; Kushnir 1994; Levitus et al. 1994; Houghton 1996; Mann and Park 1996). Mehta and Delworth (1995) present evidence that SST in the tropical Atlantic Ocean displays low-frequency variability.

* Lamont-Doherty Earth Observatory Contribution Number 5832.

Corresponding author address: Dr. Yves M. Tourre, Lamont-Doherty Earth Observatory, Columbia University, P.O. Box 1000, Rt. 9W, Palisades, NY 10964.
E-mail: tourre@ici.ldeo.columbia.edu

These characteristics of the Atlantic climate spectrum may cause analysis of time- and space-limited domain to be misleading.

Work on interannual variability in the Atlantic Ocean can be found in the seminal study of Bjerknes (1964), where large-scale SST and corresponding SLP anomalies were first identified at the interannual timescale. Bjerknes suggested that the rapid year-to-year SST variability arises from ocean–atmosphere heat fluxes forced by changing winds. He also suggested that decadal or longer fluctuations are related to changes in the ocean circulation, particularly the subtropical gyre, in response to the long-term changes of the atmospheric circulation (e.g., changes associated with the strength and location of the subtropical high). More recently, Levitus (1989) was able to identify, from hydrographic data, a weakening in the strength of the subtropical gyre in the early 1970s compared to its state in the late 1950s. Deser and Blackmon (1993) and Kushnir (1994), using longer surface datasets, found patterns of correlated variability between the atmosphere and the ocean associated with low-frequency physical mechanisms corroborating, in part, the results obtained by Bjerknes.

In general, regions with maximum sensible heat, latent heat, and momentum exchanges are not always congruent in space and time (Budyko 1982). Therefore, identifying processes associated with observed surface patterns of coherent low-frequency ocean–atmosphere variability presents a serious challenge. It has been suggested that there is interannual correlation between the tropical and extratropical North Atlantic in both the atmosphere (Nobre 1985) and the ocean (Lau and Nath 1990). The robustness of these correlations with time, as well as their frequency dependence have yet to be fully tested. For example, Houghton and Tourre (1992) and Enfield and Mayer (1997) find that the leading modes of SST interannual variability north and south of the ITCZ are uncorrelated at zero time lag. If these SST fluctuations are linked to trade wind circulation and associated changes in the strength and/or the position of the Azores and Saint Helena highs, then climate variability of the Atlantic is more complex than previously thought. The complexity in isolating climate signals is further enhanced since SST anomalies in the equatorial Atlantic Ocean are smaller than in the Pacific Ocean, and the equatorial cold tongue is much weaker (Philander 1990; Zebiak 1993; Jin 1996).

Finally, when comparing climate variability in the Pacific and Atlantic Oceans, there is evidence of an inverse relationship between SLP in the eastern Pacific and the tropical Atlantic (Covey and Hastenrath 1978), the Southern Oscillation and the SLP in the South Atlantic Ocean (Wolter 1989), and El Niño and precipitation in northeast Brazil (Caviedes 1973; Hastenrath and Heller 1977; Enfield 1996).

Most of the research involving the analyses of SST and SLP datasets from the Atlantic Ocean have focused on the North Atlantic region and it is only recently that the South Atlantic was studied (Venegas et al. 1997). In addition, almost all previous research has analyzed the data in the time domain generally by using principal component analyses or similar techniques. In an effort to better understand the spatial and temporal characteristics of Atlantic variability associated with band-limited signals, we depart from the time domain approach in this study and investigate the space–time variability of the Atlantic ocean–atmosphere system (80°N–30°S) using a joint SST and SLP analysis in the frequency domain over the Atlantic basin for a 136-yr period (1856–1991). The datasets and the method used are described in section 2. The space–time evolution patterns of SST and SLP corresponding to the dominant frequencies are described in section 3. In section 4 we discuss the results in the context of previous work and also evaluate plausible mechanisms. Summary, remarks, and conclusions are found in section 5.

2. Data and method

From the recently gridded 136-yr-long (1856–1991) global SST and SLP datasets by Kaplan et al. (1997, 1998), monthly subsets for the Atlantic domain on a 5° × 5° grid and 4° × 4° grid of SST and SLP, respectively, are obtained. Because of the sparse coverage in the South Atlantic, only data north of 30°S are analyzed in this study. Essentially, the data reduction by Kaplan et al. involves computing leading empirical orthogonal functions (EOF) from the most recent high quality data (U.K. Meteorological Office Global Ocean Surface Temperature Atlas for SST and the Comprehensive Ocean–Atmosphere Data Set for SLP). EOFs are then used for fitting a first-order linear model of time transition. The optimal estimation is obtained using EOF projection of the analyzed field in order to obtain a "reduced space." From the estimation of the available data covariance patterns, the method fills gaps, corrects sampling errors, and produces spatially and temporally coherent datasets.

The diagnostic method used for analysis is the frequency domain singular value decomposition (SVD) technique developed by Mann and Park (1994, 1996, hereafter MP94 and MP96, respectively). Time domain decomposition techniques such as principal component analysis or multichannel singular spectrum analysis are best suited for broadband features. They are poor at isolating band-limited signals that are spatially coherent, quasiperiodic, or unstable on a slowly varying noise background. In such situations the frequency domain approach is optimal (MP94). Mann and Park (1999) compare these two approaches in great detail and also demonstrate the utility of the frequency domain approach using synthetic examples.

The paradigm that the Atlantic ocean–atmosphere system exhibits spatially coherent band-limited variability on a slowly varying noise background motivated our investigation of the joint SST–SLP variability using the frequency domain approach. The goal of this paper

is to isolate dominant frequencies at which the Atlantic basin exhibits significant coherent variability and subsequently examine the corresponding spatial patterns of SST and SLP anomalies. The latter will be in general small compared to the amplitude of climate variability in the Atlantic Ocean. However, it should be kept in mind that the total amplitude, over any significant frequency band, would be an integration of the amplitudes from individual frequencies within that band. The method is briefly described below. For greater details regarding the method used, refer to MP94 and MP96.

The time series at each grid point are first transformed from the time domain to the spectral domain using the multitaper spectral method (MTM) (Thomson 1982; Park et al. 1987). At each frequency (f) for each gridpoint series, a small number (K) of independent spectral estimates are computed using K orthogonal Slepian tapers. The tapers can be thought of as a kernel or wavelet function. In addition, the tapers, being orthogonal by construction, capture independent information. The tapers average over a half-bandwidth of pf_R centered on the frequency f. Here, $f_R = 1/N\Delta t$ (Δt is the sampling interval, equal to one month in this study, and N is number of data points) is the Rayleigh frequency (the least resolvable frequency). Of the K tapers only the first $2p - 1$ tapers are usefully resistant to spectral leakage. The parameters K and p provide spectral degrees of freedom and frequency resolution, respectively. A larger p implies averaging over a bigger bandwidth, and vice versa. We choose $p = 2$ and $K = 3$, as in MP94 and MP96, which provides enough spectral degrees of freedom for a signal-to-noise ratio decomposition, while allowing reasonably good frequency resolution.

SST and SLP time series are standardized at each grid point. The anomalies are derived from long-term means (136 yr) at each point, and the standard deviations are computed at each point as well. The gridpoint series are weighted with respect to latitude. At each frequency f, K independent spectral estimates of the standardized time series are calculated as

$$Y_k^{(m)}(f) = \sum_{n=1}^{N} w_n^{(k)} x_n^{(m)} e^{i2\pi f n \Delta t},$$

where $m = 1, \ldots, M$ are the grid points (for the concatenated SST and SLP fields); $n = 1, \ldots, N$ are the time points; $k = 1, \ldots, K$ are the number of spectral estimates; and $\{w_n^{(k)}\}$ are the weights from the kth data taper. Thus, we have K spectral estimates at each gridpoint series, resulting in a matrix of size $M \times K$ at frequency f.

A complex SVD is performed on this matrix, which gives K orthonormal left and right eigenvectors representing the spatial and frequency domains of EOFs of SST and SLP anomalies, respectively, and K singular (or eigen) values representing the shared variance captured by each mode (or taper) within a given narrow-frequency band (or "local variance"). The fractional variance (or "local fractional variance") captured by each mode is then computed. The process is repeated for a number of frequencies, and a plot of the spectrum of fractional variance explained by the first mode at all the frequencies is readily obtained. Significance of peaks in the fractional variance spectrum are determined from a comparison with confidence limits obtained through a bootstrap procedure (Efron 1990). Here the fields are permuted in time to keep the spatial structure intact. One thousand permutations are generated and in each case the local fractional variance at each frequency for all the K modes is derived. From this ensemble, the 99th, 95th, 90th, and 50th percentiles are computed. There are usually a number of peaks in a given frequency window (or cluster). Consequently, the significance at a given level is obtained from the averaged highest value of fractional variance within the broader spectral band, obtained by using a local polynomial smoothing procedure (Lall et al. 1999).

When the above analysis is performed in a moving time window, an estimation of the frequency variations over time is obtained. A 60-yr moving window is used in this paper so that the evolution of the fractional variance spectrum is displayed. The left and right orthonormal eigenvectors are used to reconstruct spatial and temporal patterns at each frequency (refer to MP94 and MP96 for more details).

While the method used in this paper identifies joint SST–SLP dominant frequencies, the physical interpretation of the mechanisms associated with these frequencies can be cumbersome. This is why, prior to interpretation, the SVD joint spectrum is smoothed so that the spatial reconstructions are computed from the lead and well-separated smoothed peaks.

3. Results

The spectrum of the first singular values, and its evolution for the whole time period, are displayed in Fig. 1. For the whole time period, significant peaks at the 95% level exist in three broad bands (Fig. 1a) the quasi-biennial band (skewed around a 2.7-yr period), the interannual band (centered around periods of 3.5 and 4.4 yr), and the quasi-decadal band (skewed around an 11.4-yr period). A smoothed quasi-biennial time scale around 2.2-yr period is also significant at the 90% level. A multidecadal peak (around 50-yr period, significant at the 90% level) can also be seen in the unsmoothed curve of Fig. 1a.

The "evolutive" SVD spectrum (using a 60-yr moving window) significant above the 90% level is presented in Fig. 1b. From approximately the turn of the century until the mid 1930s there is a gap in the power of the period centered around 3.5 yr. During that same period the power of the signal centered around the 4.4-yr becomes more significant. MP96, in their joint SST–SLP analysis of the Northern Hemisphere also find significant spectral power in this time period. Other im-

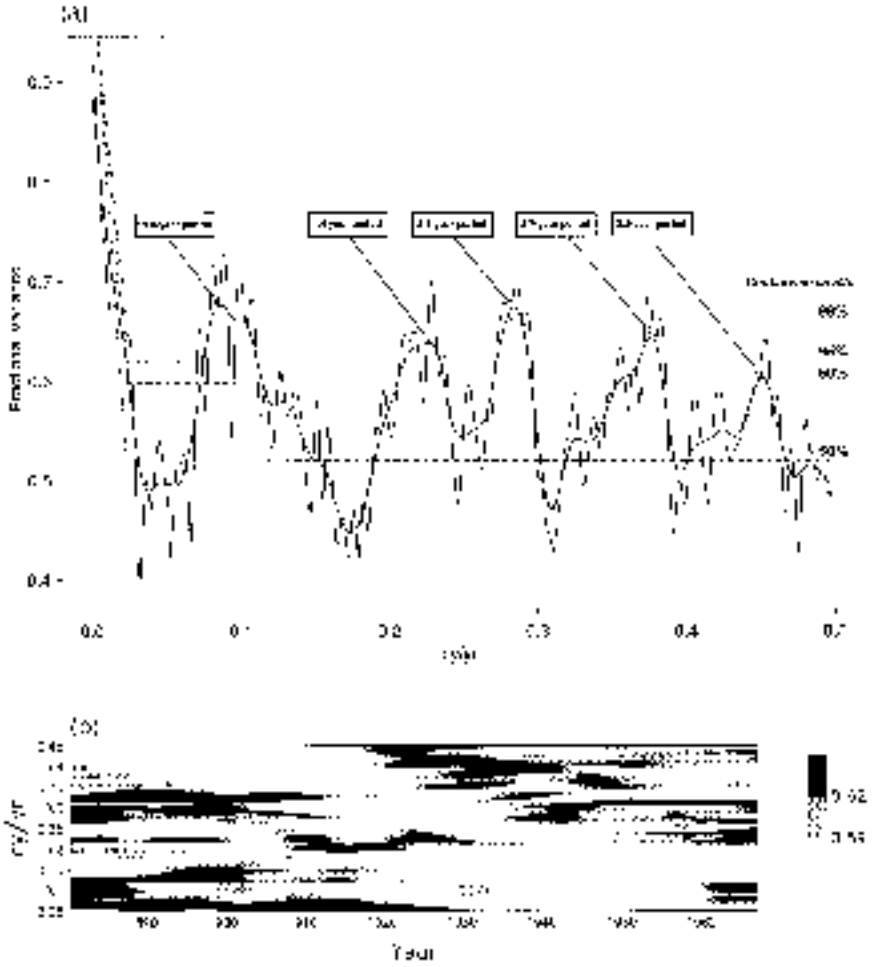

FIG. 1. (a) Spectrum of the fractional variance as a function of cycle per year explained by the first MTM/SVD joint SLP–SST mode. The thicker solid line represents a local polynomial smoothing of the frequency distribution after Lall et al. (1999). Dashed horizontal lines represent the 99%, 95%, 90%, and 50% confidence limits obtained through bootstrapping procedures after Efron (1990). (b) Frequency variations (cycle per year) as a function of time from an MTM/SVD analysis performed in a 60-yr moving time window. Only the fractional variance spectrum above the 90% confidence limit is shown in (b). The 90%–95% confidence limit is in gray (0.59–0.62 of fractional variance), while the 95% confidence limit and above is in black (over 0.62 of fractional variance).

portant features are the highly significant quasi-biennial and quasi-decadal signals around the 2.7-yr and 11.4-yr periods, respectively. The quasi-biennial signal dominates when the quasi-decadal signal is weaker and less significant. The quasi-biennial signal is conspicuous from 1920 to 1955 when the quasi-decadal signal is below the 90% confidence level. These results will be discussed in further detail in section 4e.

In the subsequent sections, joint spatial patterns of SST and SLP at the dominant frequencies, identified from Fig. 1a, are described. The evolution of the spatial patterns through half their cycle is shown in six panels. It was decided, arbitrarily, to start the first panel (Figs. 2a, 3a, 4a, and 5a) where the SLP anomalies contribute to a weakening of the Azores high. The patterns evolve through a "perfect" cycle; thus the seventh panel (not shown) is the same as the first panel with opposite polarity. The SSTs are shown in thin contours and shading and the SLPs are shown in heavy contours. The contour intervals are kept constant in all the figures for ease of comparison. The anomalies presented hereafter are in general small since they are computed over narrow bands, as explained in section 2.

a. The quasi-biennial period

Two quasi-biennial spectral peaks are centered around periods of 2.2 yr and 2.7 yr (Fig. 1a). The evolution of the spatial patterns at both these periods are very similar. Consequently, only patterns corresponding to the 2.7-

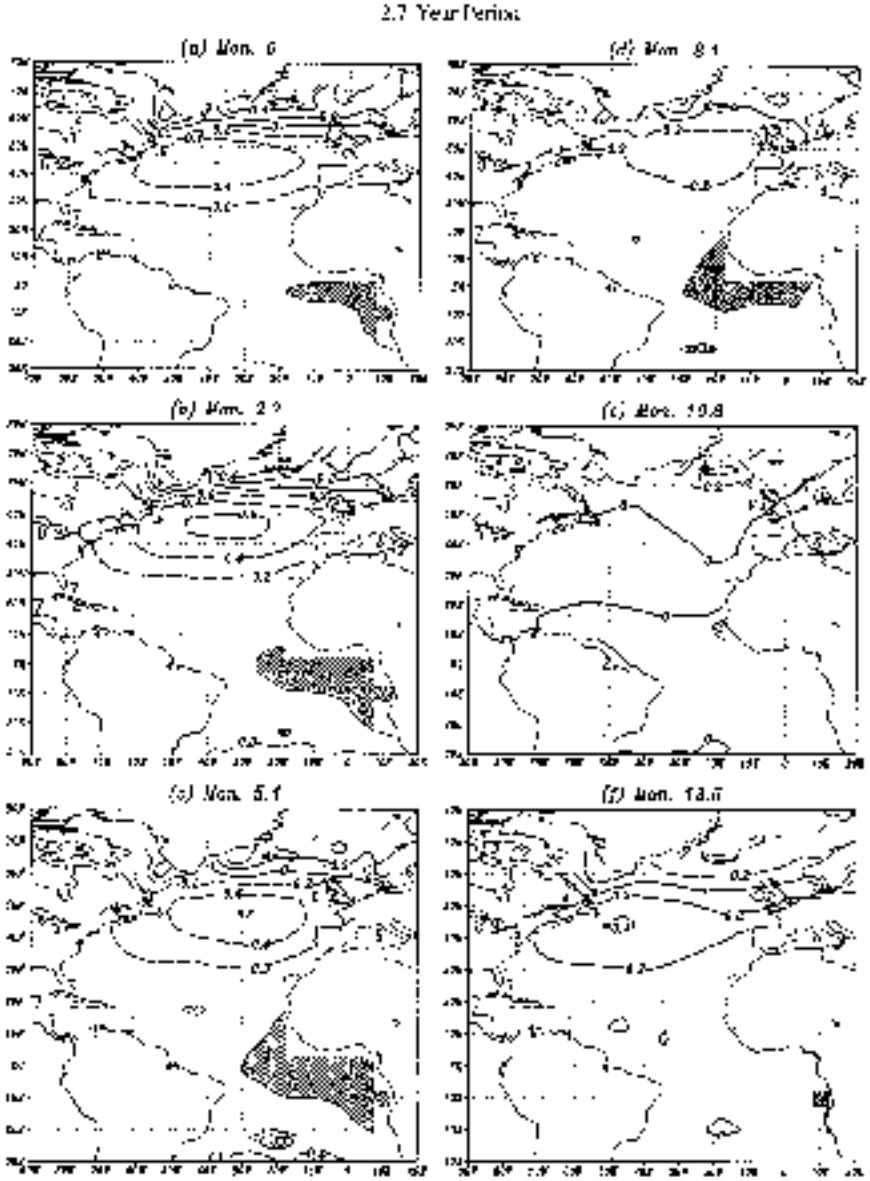

FIG. 2. Space and time evolution [top to bottom and left to right, panels (a)–(f)] of the 2.7-yr period for both SST and SLP anomalies. Only half the cycle is presented. There is a 2.7-month time difference between each frame. Thin contours (solid and dashed) represent SST anomalies (positive and negative) every 0.1°C, the zero-contour line being omitted. Shading is for values larger than 0.1°C. Thick contours (solid and dashed) represents SLP anomalies (positive and negative) every 0.2 mb.

yr period are shown in Fig. 2. The anomalies are from 0.2 mb (Fig. 2d) to 0.6 mb (Fig. 2b). The SLP anomalies form a dipole akin to the NAO. The maximum anomalous SLP occur during the part of the cycle in which weak, positive SST anomalies build up in the eastern equatorial ocean, in the regions where cold water usually dominate. The SST anomalies then expand westward along the equator and northward along the west African coastline. The tropical Atlantic Ocean is alternatively warmer or colder (up to 0.2°C) every 16 months. The maximum expansion of SST anomalies in the Tropics (Fig. 2c) occurs 3 months after maximum negative SLP anomalies between Newfoundland and western Europe (Fig. 2b).

b. The interannual bands

Two distinct spectral peaks centered around 3.5- and 4.4-yr periods are identified at the interannual timescales. These frequencies capture more than 60% of the

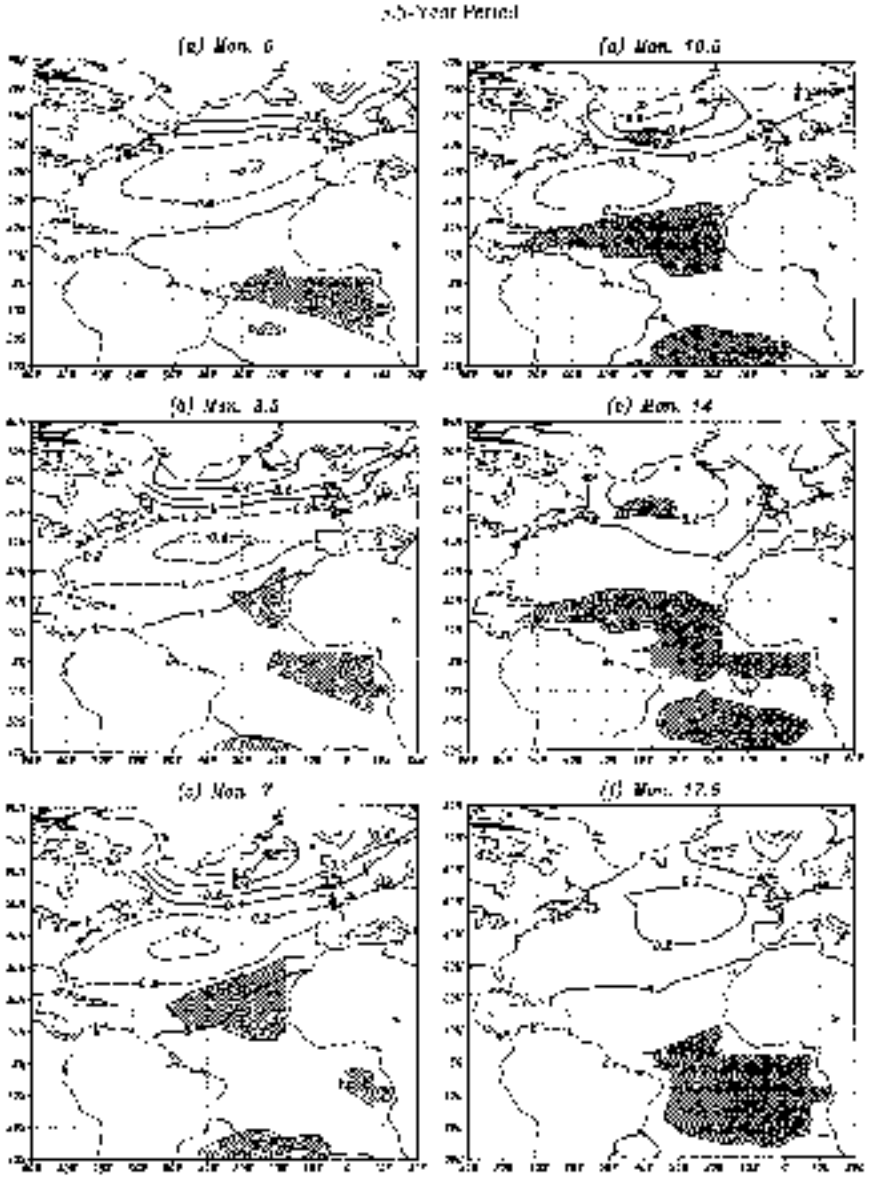

FIG. 3. Space and time evolution (top to bottom and left to right, panels (a)–(f)) of the 3.5-yr period for both SST and SLP anomalies. Only half the cycle is presented. There is a 3.5-month time difference between each frame. Contouring convention is the same as for Fig. 2.

fractional variance in a narrow band centered around them (see Fig. 1a).

1) The 3.5-yr period

Figure 3 shows the evolution of the anomalies for half this period. Maxima of SLP anomalies in the North Atlantic form a dipolelike pattern akin to the NAO. The largest anomalies (0.6 mb) are identified first in the Denmark Strait and then west of the Azores (Figs. 3c and 3d). The anomalies persist for approximately half a year with little motion and then the pattern mentioned above collapses (Fig. 3e). The strongest anomalous SLP gradient is found between 45°–55°N and 20°–50°W (Figs. 3b and 3c). In the tropical Atlantic, SLP anomalies are weaker (0.1 mb).

In the North Atlantic Ocean, SST anomalies are rather weak despite the strong SLP gradient mentioned above (Fig. 3d). Weak SST anomalies (0.1°C) at 50°N and 30°–40°W occur 3–6 months after the maximum anomalous SLP gradient. More specifically, positive SST anomalies peak (0.1°–0.2°C) between 50° and 55°N, and between 10° and 20°N (Figs. 3d and 3e).

SST anomalies appear along the West African coastline, in the region where climatological features such as the cold Canaries current and coastal upwelling dom-

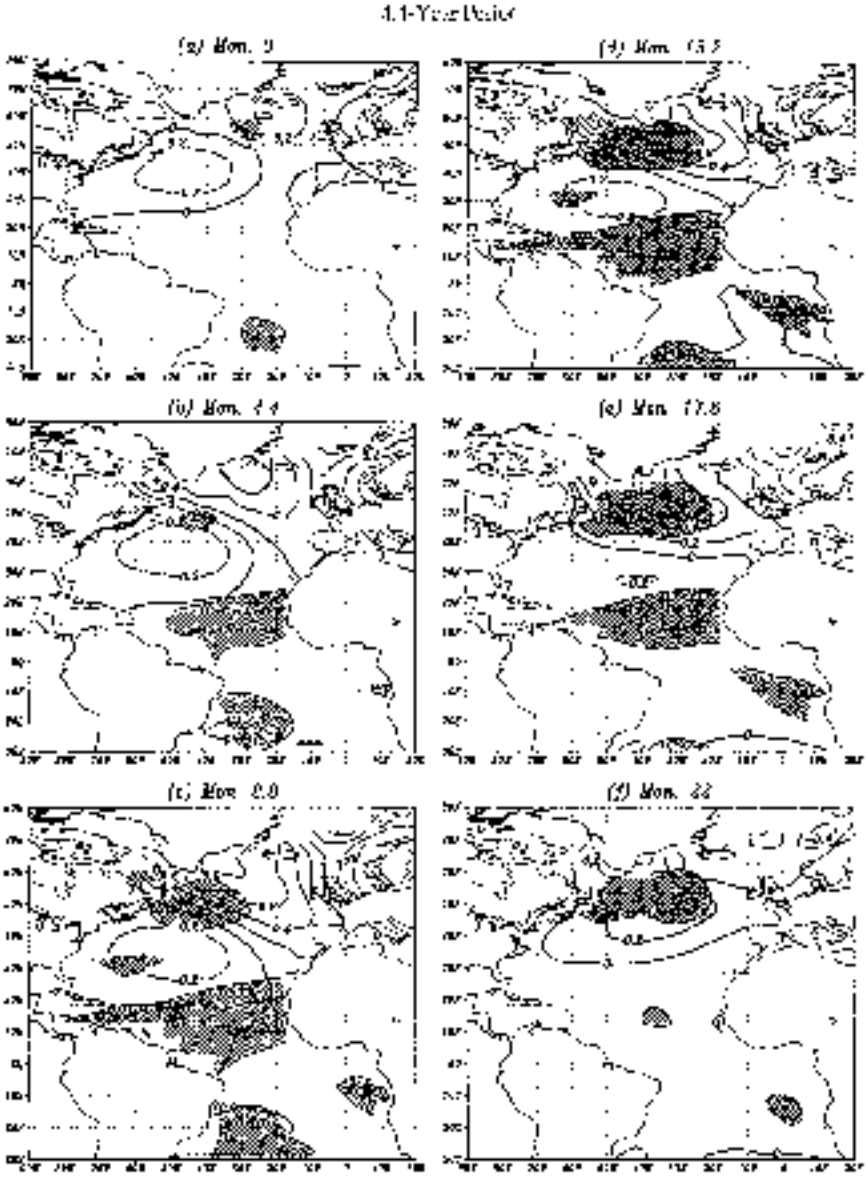

FIG. 4. Space and time evolution [top to bottom and left to right, panels (a)–(f)] of the 4.4-yr period for both SST and SLP anomalies. Only half the cycle is presented. There is a 4.4-month time difference between each frame. Contouring convention is the same as for Fig. 2.

inate (Fig. 3b). SST anomalies along the Senegalese coastline occur when SLP anomalies contribute to a weakening of the North Atlantic SLP dipole. From there the anomalies expand westward between approximately 10° and 20°N, consistent with the path of the North Equatorial Current, and then southward between the West African coastline and 30°W. At 10°S a merging occurs with anomalies moving northward from the South Atlantic Ocean (Fig. 3e). Finally, the anomalies find their way into the gulf of Guinea following the mean path of the North Equatorial Counter Current and the Equatorial Undercurrent.

2) The 4.4-yr period

Figure 4 shows the evolution of the spatial patterns associated with half this period. The largest SLP anomalies are identified between Iceland and the southern tip of Greenland (0.6–0.8 mb), and at 35°N between 35° and 65°W (0.2 mb, Fig. 4b), they persist for approximately ¾ of the cycle with little motion. To the south between 25° and 35°N and between 30° and 50°W, the anomalies collapse (25°N, 40°W, Fig. 4e), a year later. In the western North Atlantic Ocean, maximum positive SLP anomalies are found over southern Greenland (Fig. 4c).

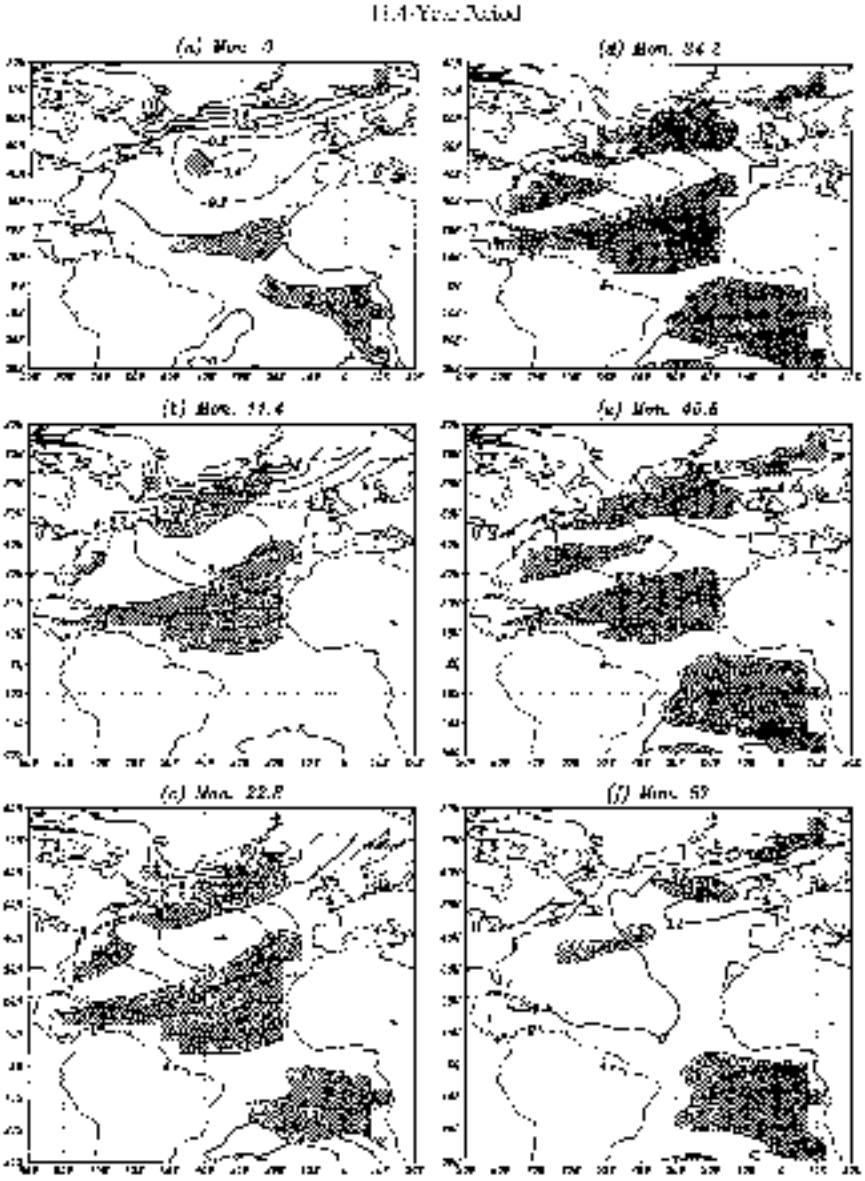

FIG. 5. Space and time evolution [top to bottom and left to right, panels (a)–(f)] of the 11.4-yr period for both SST and SLP anomalies. Only half the cycle is presented. There is a 11.4-month time difference between each frame. Contouring convention is the same as for Fig. 2.

Positive SST anomalies (up to 0.3°C) appear in the 40°–60°N zonal band, where the SLP gradient is such that westerly winds are weakened (Figs. 4c and 4d). This could reduce storm activity during winters occurring during the cycle. Along 30°–40°N negative SLP anomalies are found 15–20 degrees of longitude east of the negative SST anomalies (Figs. 4c and 4d). Peak SST anomalies lag peak SLP anomalies by several months. Contemporaneously, positive SST anomalies (0.1°–0.3°C) are the dominant feature in the North Tropical Atlantic Ocean (Figs. 4c, 4d, and 4e) where northeasterly winds must be weaker. In the South Tropical Atlantic, negative (positive) SST anomalies appear offshore of central Africa (Gabon, Congo, and Angola, Figs. 4c). Subsequently, these anomalies expand westward (Figs. 4d and 4e).

c. *The quasi-decadal period*

The prominent quasi-decadal peak around the 11.4-yr period can be seen in Fig. 1a. The fractional variance captured at this frequency is significant at the 99% level. The spatial patterns associated with the quasi-decadal band are displayed in Fig. 5.

In the North Atlantic the SLP anomaly patterns are reminiscent of the NAO pattern. An out-of-phase re-

lationship also occurs between the areas where the subtropical anticyclones in both hemispheres are found the Azores high to the north and the Saint Helena high to the south. The difference in signs between the SLP anomalies to the north and the subtropical highs leads to the conclusion that quasi-decadal variability is also present in the winds at all latitudes. In Fig. 5, where the maximum SLP anomalous gradient is visible (Figs. 4a, 4b, and 4c), it can be inferred that when the westerlies between 50° and 65°N are weaker than normal, the northeasterly trades are also weaker than normal. At the same time the southeasterly trades are stronger than normal.

An in-phase relationship between SST anomalies in the 50°–60°N zonal band and the North Tropical Atlantic Ocean (north of the mean position of the ITCZ) is readily seen (Figs. 5b, 5c, and 5d). Furthermore, a coherent east–northeast oriented pattern of SST anomalies is found just south of the Gulf Stream extension and along the North Atlantic Current (Figs. 5a–f). SST anomalies are also found in the vicinity of the North Athantic drift (Fig. 5a with reversed polarity).

SST anomalies in the North Atlantic Ocean, north and south of the Azores high have the same polarity. In contrast SST anomalies have opposite polarity north and south of the mean position of the ITCZ (Fig. 5d). This distribution of SST anomalies fits well with the in-phase relationship between midlatitude westerlies and northeasterly trade winds and the out-of-phase relationship of Atlantic northerly and southeasterly trade winds on this timescale, as previously discussed. The evolution of tropical SST during the decadal cycle is thus marked by the appearance of a seesaw pattern of SST during the growth phase of the pattern.

4. Discussion

All spatial patterns corresponding to the four frequencies begin arbitrarily (Figs. 2–5), with a weaker than normal Azores anticyclone and a weaker than normal Icelandic low. All of these SLP anomalies contribute to a negative NAO index at the beginning of each cycle. In this section we compare our results with relevant previous work and also discuss possible physical mechanisms involved with the dominant signals that we have identified.

a. The quasi-biennial period

Wagner (1971), in an analysis of a 66-yr Northern Hemisphere SLP dataset (north of 20°N), and other investigators (e.g., Landsberg et al. 1963), identified tropospheric quasi-biennial signals or "pulses." Wagner concluded that the spectral power in a band centered at a period of around 2.5-yr displayed maximum amplitude in both SST and SLP. The maxima associated with the spectral band were located near the centers of the Icelandic low and the Azores high during winter. These results were corroborated later by Angell and Korshover (1974), who also argued that the quasi-biennial fluctuations and their different frequencies are linked to the southwest–northeast movement of the "centers of action," that is, the Icelandic low and the Azores high. They showed that the Azores high becomes weaker when displaced southward. A quasi-biennial oscillation was subsequently identified in the temporal record of the NAO by van Loon and Rogers (1978). More recently, quasi-biennial signals were identified in SLP over the Northern Hemisphere (Trenberth and Shin 1984); SLP, surface wind, and air temperature data from the north Atlantic Ocean (Gordon et al. 1992; Deser and Blackmon 1993); and from global analysis of air temperature and SST (MP94).

In our analysis we find two spectral peaks in the vicinity of the 2.5-yr period. The evolution of SLP anomalies in the North Atlantic is consistent with the results obtained by Angell and Korshover (1974). The contribution of the biennial signal to SLP variability there is particularly evident after ~1920 (Fig. 1b). The shape and evolution of the patterns of tropical SST anomalies from the Angolan coastline (Figs. 2a–d) seems to indicate that the anomalous local currents (e.g., the South Equatorial Current, or SEC) play a preponderant role. It is interesting to note that Konda et al. (1996), using bandpass-filtered biennial variations of SST obtained from satellite data, concluded that SST evolution in the tropical Atlantic Ocean is primarily controlled by lateral heat transport and not air–sea heat fluxes. Negative SLP anomalies from 60°N to 30°S are associated with a warmer tropical ocean. The fact that the maxima in SLP and SST anomalies are far apart deserves further investigation.

b. The interannual band

During the last two decades there has been considerable evidence of a relationship between the negative phase of the Southern Ocean Index and equatorial Atlantic warm events (Covey and Hastenrath 1978; Hastenrath et al. 1987; Wolter 1989; among others). Modeling experiments have established links between the intensity of the tropical Atlantic trades and the ENSO phenomenon (Tourre et al. 1985; Carton and Huang 1994; Delecluse et al. 1994). Zebiak (1993) discussed the importance of meridional SST gradients in the Atlantic domain and its association with tropical Atlantic Ocean circulation. Curtis and Hastenrath (1995), from a composite study, describe the evolution of meridional SST gradients in the tropical Atlantic Ocean. Wagner (1996) proposed physical mechanisms associated with the tropical meridional SST gradient. Spectral peaks around 5-yr period were found by Venegas et al. (1997) in the South Atlantic from a joint analysis of SST–SLP in the time domain, based on the most recent 50 yr of data. They associate this variability with a meridional displacement of the ITCZ and the Saint Helena anti-

cyclone (the Southern Hemisphere subtropical high). Sperber and Hameed (1993) identify a 3.6-yr period in the northern tropical Atlantic SST, which they argue is one of the timescales at which the Walker circulation interacts with the tropical Atlantic circulation and modulates the track of the Atlantic ITCZ. Peterson and White (1998) identified an Antarctic circumpolar wave, with a period of 4–5 yr, transmitting climate anomalies in the Southern Oceans, including the South Atlantic Ocean.

1) The 3.5-yr period

For the 3.5-yr period it is found that, in the North Atlantic, SST anomalies are rather weak even in the presence of large SLP anomalous gradient. The SLP anomalies are such that northeasterly trade winds are weaker in the northern tropical Atlantic Ocean and along the northwest African coastline. When a similar analysis is performed globally (not shown) we found that for approximately the same 3.5-yr period, the patterns displayed in Fig. 3a correspond to the time when a fully developed El Niño exists in the eastern Pacific. The southeasterly trade winds in the equatorial Atlantic will be at their peak strength, the negative SST anomaly being the largest in the equatorial Atlantic. The ITCZ will then be found farther north with weaker coastal upwelling and reduced heat loss between 10° and 20°N (Curtis and Hastenrath 1995). At the equator and at the beginning of the arbitrarily defined cycle (Fig. 3a), negative SST anomalies and weak positive SLP anomalies are observed. Tropospheric subsidence and hydrostatic adjustment of the atmosphere to cold SST (Covey and Hastenrath 1978; Lindzen and Nigam 1987) will both increase SLP. The positive SST anomalies in the South Atlantic Ocean (at 30°S) expand equatorward following geostrophic flow patterns of the upper ocean (Reid 1989; Stramma 1991) and merge (west of 20°W) with positive SST anomalies from the north. These anomalies are reinforced by Ekman downwelling in those regions (Curtis and Hastenrath 1995). The merging on the western tropical basin might be due to a tendency for the ITCZ to create, farther east, an initial potential vorticity barrier that inhibits direct flow along the thermocline layer from subtropical region toward the equator (Lu and McCreary 1995). From there they propagate east–southeastward (Figs. 3a, 3b, and 3c, all with reverse polarity). This anomalous propagation follows very closely the anomalous gradient of the sea level topography computed from the oceanic geopotential thickness for the 0–1000-m layer (Levitus and Oort 1977). A similar movement is noticed in the heat storage anomalies associated with the ENSO phenomenon (Tourre and White 1999, manuscript submitted to *J. Climate*).

The tendency for a warmer northern tropical Atlantic Ocean during ENSO peaks, as in the 1980s, is seen in the global rotated EOF analysis of Tourre and White (1995). To gain further insight about this relationship, we compute the coherence and phase between the SST NINO3 time series (representative of the Pacific ENSO) and reconstruct time series averaged over grid points along the equatorial Atlantic. We find the largest significant coherence of 0.65 (99% level of confidence) at around 12-month lag, for the 3.5-yr period. This seems to suggest, for example, that the 3.5-yr signal contributes to a weakening of the Azores high (Figs. 3a–d) and that about one year after a fully developed El Niño in the eastern Pacific, a warming of the equatorial Atlantic Ocean is noticeable, with maximum SST anomalies (up to 0.2°–0.3°C) occurring in the Gulf of Guinea (Hisard 1980). This corroborates well with results by Philander (1990), Tourre and White (1995), and Latif and Barnett (1995). During the Atlantic warm event of 1984, after the 1982–83 "ENSO of the century" in the Pacific Ocean, a South Equatorial Counter Current (SECC) was monitored (Hisard and Henin 1987). An eastward propagation of SST anomalies was observed during the Atlantic warm event of 1984 (Henin and Hisard 1987; Reverdin and McPhaden 1986). It was also concluded that during this period positive SST anomalies between the equator and 10°S and east of 20°W were indicative of a weaker SEC and a weaker Benguela Current system (Carton and Huang 1994; Philander 1986; Reverdin et al. 1991).

The above arguments reinforce the idea of a specific Atlantic response to the Pacific ENSO signal as transferred through the "atmospheric bridge" as suggested by Lau and Nath (1996). The reason for the signal to be transmitted at that particular frequency and the potential role played by the atmosphere in the midlatitudes remain unclear.

2) The 4.4-yr period

The evolution of the negative SST anomalies south of the ITCZ indicates the presence of stronger southeasterly trade winds (Figs. 4c and 4d). The lack of SLP data south of 30°S does not permit us to isolate a definite joint SLP anomaly pattern there. SLP anomalies in the vicinity of the Azores high are negative, but they are somewhat weaker when compared with SLP anomalies for the 3.5-yr period in the same region (Figs. 3c and 4c). South of the Azores high weaker northeasterly and stronger southeasterly winds, compared to the 3.5-yr period, further tend to displace the ITCZ northward. As a result of the stronger local meridional winds, coastal upwelling gets enhanced along the Angolan coastline and is extended far westward (Shannon et al. 1986), while the strength of the Angola gyre (Gordon and Bosley 1991) tends to be reduced. When the southeasterly trade winds are relaxed, a warming occurs in the same region primarily due to heat redistribution by the SEC and SECC (Philander and Pacanowski 1981). Finally, SST anomalies are found farther north in both hemispheres in regions where there is also maximum Ekman drift in the mean (Mellor et al. 1982; Arnault 1987).

Similar conclusions from modeling studies were argued by Zebiak (1993) and Carton and Huang (1994).

c. Comparisons of the two interannual periods

From the way the interannual cycles are reconstructed in this paper and from a global analysis [not shown and already mentioned in section 4b(1)], it can be deduced that the atmospheric linkage between the eastern Pacific and Atlantic Oceans is increased during the prominent 3.5-yr period of the ENSO phenomenon. This is, for example, when negative SLP anomalies are found in the eastern Pacific, negative SLP anomalies are found in the vicinity of the Azores high, and the SLP increases in the equatorial and South Atlantic through presumably tropospheric subsidence. Interestingly enough, when we performed additional spectrum analyses of the winter NAO and its two components, the Azores high and the Icelandic low, a significant interannual signal (90% confidence level) is centered around 3.5 yr. The linkages between the eastern Pacific SLP anomalous field associated with ENSO and the intensity of the Azores high could be associated with "an equivalent barotropic wave-like response in the North Pacific–North American" region as mentioned by Lau and Nath (1996). Lau and Nath were also able to associate warm ENSO events with a dipolelike SST pattern in the western North Atlantic (negative SST anomalies along the northeastern seaboard of North America associated with negative anomalies in latent and sensible fluxes). More work remains to be done in this domain.

The SST evolution in the tropical Atlantic is different for the 3.5- and 4.4-yr periods. In the southeast Atlantic, SST anomalies propagate and/or expand in opposite directions, that is, southeastward for the 3.5-yr period and northwestward for the 4.4-yr period. A fundamental difference between the two cycles is that colder equatorial SST are associated with higher tropical SLP for the 3.5-yr period, while for the 4.4-yr period this relationship breaks down. Since the joint SST–SLP evolution north of the ITCZ display similarities between the two cycles, the difference in the SST evolution south of the ITCZ must be linked to independent local atmospheric and oceanic conditions in the South Atlantic Ocean.

It is well known that the position of the ITCZ in the tropical Atlantic is associated with local conditions, such as the intensity of the northwest African heat low and the strength and position of the Saint Helena anticyclone. In the ocean these changes correspond to changes in the strength of the south subtropical gyre. The position of the ITCZ displays seasonal, interannual, and lower-frequency variability. For example, when spectral analysis is performed on time series that depict the anomalous location of the ITCZ, the two intermediate frequencies discussed in this paper are clearly identified (not shown). Remote forcing, including ENSO, also influence the position of the Atlantic ITCZ. It has been shown that the latitude of the ITCZ is determined by the meridional SST gradient, the meridional SLP gradient, and the relative intensity of the trades, northeasterly versus the southeasterly (Covey and Hastenrath 1978; Hameed et al. 1997; Wagner 1996; Wainer and Soares 1997). We propose that the differences in the SST evolution south of the ITCZ between the 3.5- and 4.4-yr periods reside in the relative difference in the strength of the trade winds system and the changes in the oceanic circulation due to both local and remote forcing. For both cycles, when the NAO is weaker the northeasterly trade winds are weaker. Accordingly the ITCZ is found farther north. Furthermore, when El Niño is fully developed there is an indication of positive equatorial SLP anomalies (Figs. 3a–c). For the 4.4-yr period (Fig. 4) weak positive SLP anomalies are found farther south (Figs. 4d and 4e) and could be associated with a stronger and/or northward displacement of the Saint Helena anticyclone. This movement has been mentioned by Venegas et al. (1997). Resulting equatorial warming is then influenced by local conditions with weaker southeasterly trade winds. From the south, SST anomalies could also penetrate the Tropics by entering the Benguela Current system and subsequent northward spreading from the SEC. Finally the possible link with the 4–5-yr period of the Antarctic circumpolar wave and northward Ekman layer flow propagation identified by White and Peterson (1996) and Peterson and White (1998 deserves further investigation.

d. The quasi-decadal period

The Atlantic climate variability is characterized by a strong coherence associated with this cycle. Deser and Blackmon (1993) find that SST quasi-decadal variability is associated with the western Atlantic oscillation, a geopotential pattern in the upper troposphere (Wallace and Gutzler 1981). Molinari et al. (1997) were able to identify the same timescale variability in the subsurface temperature (down to 400 m) in the midlatitudes of the western north Atlantic Ocean. From coupled-model runs, Grötzner et al. (1998) identify low-frequency variability of around a 17-yr period in their joint SST–SLP of the Atlantic basin and attribute it to unstable air–sea interactions revolving the subtropical gyre and the NAO. In their experiment the ocean responds to low-frequency wind stress curl variations and serves as a memory in the coupled system. The intensity of the Gulf Stream extension and the subtropical gyre respond accordingly and keep the coupled system oscillating. Similar findings were made by Hansen and Bezdek (1996) and Halliwell (1995). In the subtropical gyre, the latent heat flux is found to force quasi-decadal SST anomalies (Cayan 1992). North of 30°N the SST anomalies closely follow the mean transport stream function derived from wind stress and subsurface density fields (Mellor et al. 1982). The amplification of SST anomalies to the north of 50°N, the region where the barotropic flow associated with the subpolar gyre (Hogg et al. 1986), separates

from the Sargasso gyre. Sutton and Allen (1997) find a similar evolution in SST anomalies when they analyzed SST for a shorter time period (1945–89).

In our joint SST–SLP analysis, the spatial distribution of SLP anomalies is a reminder of the NAO standing index characteristics. The joint SST and SLP patterns associated with an 11.4-yr period (as shown in this paper) points to a strong midlatitude NAO–SST linkage and a strong tropical–extratropical connection at decadal timescales. This result emphasizes a timescale defined by the ability of upper-ocean anomalies to persist, even after the atmospheric anomalies decay, and during which ocean–atmosphere interaction is maintained on the Atlantic basin scale.

Hurrell (1995), Halliwell (1995), and Kushnir (1996) suggest that positive SST anomalies in the westerlies and trade wind belts appear simultaneously when the anomalous SLP gradient is decreased. This is corroborated by the relative distribution of SST and SLP anomalies in Fig. 5.

In the tropical Atlantic, quasi-decadal variability is associated with an out-of-phase relationship in the SST to the north and south of the ITCZ. This is consistent with previous analyses from Houghton and Tourre (1992) and Servain (1991), who identified a decadal timescale for an SST tropical "dipole index." Mehta and Delworth (1995) mention that SST variability south and north of the ITCZ occurs at timescales between 8 and 11 yr. Recently, Chang et al. (1997), using a hybrid coupled general circulation model, show that a dipole structure with a decadal timescale can be attained through unstable thermodynamics between wind-induced heat fluxes and SST anomalies. Northern and southern tropical components of the SST anomaly structure might be associated with the same mechanisms, but a true dipole structure is retained only for a relatively short time period (for at most 2 yr) in the quasi-decadal evolution. This is consistent with our results. When SVD and cross-spectral analyses are performed, with the NAO and subtropical SST normalized time series, significant coherence is found north and south of the equator. Nevertheless, the cross spectral analysis between SST in the two regions identified in Fig. 5d reveals very little coherence (Rajagopalan et al. 1998). This leads us to believe that SST in the two subtropical regions are independently coherent with NAO (Kushnir et al. 1998).

The trade winds are out of phase on this timescale since the subtropical anticyclones are also out of phase. The meridional SST gradient across the ITCZ associated with the decadal pattern has a profound effect on the northeast Brazil and Sahelian rainfall (Hastenrath and Heller 1997; Mechoso et al. 1990; Sperber and Hameed 1993; Wainer and Soares 1997).

e. *Comparison of quasi-biennial and quasi-decadal periods*

As shown in Fig. 1b, the statistical significance of the quasi-biennial and quasi-decadal bands varies with time. This was first mentioned by Kutzbach (1970). In particular, we can note from this figure that, when the quasi-biennial period was significant during the 1920–55 period, the quasi-decadal period was much less prominent. The interannual period, especially the 3.5-yr signal also seems to be less significant during this period. Gu and Philander (1995) note that between 1915 and 1950 the intensity of the Southern Oscillation was relatively small and increased rapidly thereafter. Similar observations were found by Rajagopalan et al. (1997) in their analysis of Darwin SLP data. The relationship, as a function of time, between the quasi-biennial and quasi-decadal periods is still unclear. According to Hurrell and van Loon (1996), the NAO "standing index" has exhibited considerable variability at quasi-biennial and decadal timescales during the past 130 yr. This is not the case in Fig. 1b, where the biennial signal is not significant prior to 1920. They also show that the NAO decadal variability becomes more pronounced after the 1950s. Similarity and differences between their results and ours could be due to several facts: 1) our study emphasizes the evolution of joint (both SST and SLP) spatial patterns as opposed to amplitudes of individual standing indices such as the NAO index for the North Atlantic only; 2) our analysis emphasizes joint coherent frequency bands and not necessarily spectral power, in which the power is shared between two fields over the entire Atlantic domain; 3) our analysis is based on monthly data as opposed to the winter time values of the NAO index used by Hurrell and van Loon (1996). Indeed, a moving-window spectrum on monthly time series of the NAO index (not shown) reveals a prominent quasi-decadal band prior to ~1920 as in Fig. 1b. We can infer from Rogers (1984) and Hurrell (1995) that between ~1920 and ~1960 there was a downward trend in the NAO index. Also, during the 1920–60 interval both the Azores high and the Icelandic low moved southwestward (Glowienka 1985). During that period the SLP over the Greenland–Iceland regions gradually increased (Rogers 1984) and the winter storm tracks in the North Atlantic were found farther south (Tinsley 1988). This year interval is roughly related to the North Atlantic "warm period" identified by Kushnir (1994). The physical link between those observations and the concomitant changes in frequency characteristics of the joint SST–SLP patterns is not clear at this time. In a joint SST–SLP spatio-temporal analysis for the Northern Hemisphere, MP96 found that the quasi-decadal signal appeared as a distinctly cold-season phenomenon while the quasi-biennial signal is significant during both independent warm and cold seasons and stronger during the cold season. The effect of seasonality, while studying tropical–extratropical interactions for the entire Atlantic Ocean, needs further research.

In this paper it is shown that there is a relationship between localized SLP variations and dominant cycles in the joint SST–SLP variability in the North Atlantic. Generally, during the period when the NAO index di-

minishes, the quasi-biennial cycle is enhanced, which indicates a possible quasi-decadal modulation on shorter timescale variability. It is also believed that while NAO variability is tightly linked with SST variability (e.g., Kushnir 1994), the biennial variability as described in this analysis is largely atmospheric (compare the amplitudes of SST and SLP anomalies in Fig. 2). This is beyond the scope of this paper.

5. Summary

Five significant frequency bands for the joint SST–SLP evolution are identified in the Atlantic basin. They range from the quasi biennial to the quasi decadal. Two quasi-biennial bands are centered around 2.2- and 2.7-yr periods; two interannual bands are centered around 3.5- and 4.4-yr periods; the fifth band at the quasi-decadal frequency is centered around 11.4-yr time period. The spatial patterns corresponding to the five periods display large SLP variability in the North Atlantic. With the quasi-decadal period, the SLP patterns and their time evolution are not only linked with the NAO, but also with an out-of-phase relationship between the subtropical anticyclones in both hemispheres. This indicates a dominant quasi-decadal variability in the Atlantic Hadley circulation.

The five significant frequency bands are all associated with tropical warming with different intensities and evolution along the equatorial wave guide. For the quasi-biennial bands the entire tropical Atlantic gets simultaneously warmer (colder). For the other three bands there are out-of-phase relationships north and south of the mean position of the ITCZ. For the quasi-decadal band, this relationship leads to a short-lived dipole structure due to independent SST time evolution north and south of the ITCZ. The 3.5-yr band displays eastward evolution along the equator and seems to be linked to the Pacific ENSO through the atmosphere (warm/cold Atlantic events lag the Pacific by 15–18 months). The warm (cold) events associated with the 4.4-yr band are weaker, propagate westward along the equator, and seem to be depending upon local Atlantic conditions such as the locus of the ITCZ.

From a modeling study, Grötzner et al. (1996) suggested that the Atlantic decadal climate cycle is a coupled ocean–atmosphere phenomenon as it is in the Pacific (Latif and Barnett 1994; Tourre et al. 1999). The apparent difference between the two low-frequency signals in the Atlantic and the Pacific must then be attributed to the size difference of the two basins and the dominance of the NAO in the North Atlantic. The latter implies a potential for atmospheric feedback. It is interesting to note that while Wohlleben and Weaver (1995) identified an interdecadal signal in the SST of the subpolar North Atlantic gyre, Houghton (1996) found a quasi-decadal fluctuation in the upper portion of the Labrador Current, where vertical mixing is weaker due to freshwater input from the Arctic (Reverdin et al. 1997).

The relationship between the dominant joint evolution of SST–SLP and their appropriate frequencies requires further investigation (with additional datasets including subsurface temperature, salinity, and precipitation). For example, preliminary reconstruction of the joint SST–SLP patterns corresponding to the 50-yr peak in Fig. 1b (not shown) seems to be consistent with the results from Delworth et al. (1993) and Kushnir (1994), suggestive of variability in thermohaline circulation as a plausible driving mechanism at this timescale. Isolating the main physical mechanisms involved by comparing results from diagnostic analyses with modeling output (reproducibility) will have immediate predicting application (Pittalwala and Hameed 1991). Nevertheless, complexity could arise since the different signals (their relative intensity, stability, and evolution) modulate each other, as evidenced in this paper, when the quasi-biennial and the quasi-decadal signals are compared (Fig. 1b). Finally, more insight can be gained on the mechanisms associated with the patterns presented in this study by exploring the role of seasonality.

Acknowledgments. The authors would like to express their appreciation to Mike Mann for the numerous fruitful discussions they had with him. Those discussions contributed invaluably to this paper. We are grateful, as well, for the suggestions made by the two anonymous reviewers.

Y. M. Tourre and B. Rajagopalan were supported in this study by NOAA Grant UCSI0-1077541D/NA47GP0188. Y. Kushnir was supported by NOAA Grant NA56GP0161.

REFERENCES

Angell, J. K., and J. Korshover, 1974: Quasi-biennial and long-term fluctuations in the centers of action. *Mon. Wea. Rev.*, 102, 669–678.

Arnault, S., 1987: Tropical Atlantic geostrophic currents and ship drifts. *J. Geophys. Res.*, 92, 5076–5088.

Barnett, T. P., M. Graham, M. A. Cane, S. E. Zebiak, S. C. Dolan, J. J. O'Brien, and D. Legler, 1988: On the prediction of the El Niño of 1986–1987. *Science*, 241, 192–196.

Bjerknes, J., 1964: Atlantic air–sea interaction. *Advances in Geophysics*, Vol. 10, Academic Press, 1–82.

Budyko, M. I., 1982: *The Earth's Climate Past and Future*. Academic Press, 307 pp.

Cane, M. A., and S. E. Zebiak, 1985: A theory for El Niño and the Southern Oscillation. *Science*, 228, 1085–1087.

——, ——, and S. C. Dolan, 1986: Experimental forecasts of El Niño. *Nature*, 321, 827–832.

Carton, J. A., and B. Huang, 1994: Warm events in the tropical Atlantic. *J. Phys. Oceanogr.*, 24, 888–903.

Caviedes, C. N., 1973: Secas and El Niño two simultaneous climatic hazards in South America. *Proc. Assoc. Amer. Geogr.*, 5, 44–49.

Cayan, D. R., 1992: Latent and sensible heat flux anomalies over the northern oceans: Driving the sea surface temperature. *J. Phys. Oceanogr.*, 22, 859–881.

Chang, P., L. Ji, and H. Li, 1997: A decadal climate variation in the

tropical Atlantic Ocean from thermodynamic air–sea interactions. *Nature*, 385, 516–518.

Chen, D., S. E. Zebiak, A. J. Busalacchi, and M. A. Cane, 1995: An improved procedure for El Niño forecasting. *Science*, 269, 1699–1702.

Covey, D., and S. Hastenrath, 1978: The Pacific El Niño phenomenon and the Atlantic circulation. *Mon. Wea. Rev.*, 106, 1280–1287.

Curtis, S., and S. Hastenrath, 1995: Forcing of anomalous sea surface temperature evolution in the tropical Atlantic during Pacific warm events. *J. Geophys. Res.*, 100, 15 835–15 847.

Delecluse, P., J. Servain, C. Levy, K. Arpe, and L. Bengtsson, 1994: On the connection between the 1984 Atlantic warm event and the 1982–1983 ENSO. *Tellus*, 46A, 448–464.

Delworth, T., S. Manabe, and R. J. Stouffer, 1993: Interdecadal variations of the thermohaline circulation in a coupled ocean–atmosphere model. *J. Climate*, 6, 1993–2001.

Deser, C., and M. L. Blackmon, 1993: Surface climate variations over the North Atlantic Ocean during winter 1900–1989. *J. Climate*, 6, 1743–1753.

Efron, B., 1990: The jackknife, the bootstrap and other re-sampling plans. Memo. 38, Society for Applied and Industrial Mathematics, 92 pp. [Available from SIAM, 3600 University City Science Center, Philadelphia, PA 19104.]

Enfield, D. B., 1996: Relationship of inter-American rainfall to tropical Atlantic and Pacific SST variability. *Geophys. Res. Lett.*, 23, 3305–3308.

——, and D. A. Mayer, 1997: Tropical Atlantic SST variability and ENSO. *J. Geophys. Res.*, 102, 929–945.

Glowienka, R., 1985: Studies on the variability of Icelandic Low and Azores High between 1881 and 1983. *Beitr. Phys. Atmos.*, 58, 160–170.

Gordon, A. L., and K. T. Bosley, 1991: Cyclonic gyre in the tropical south Atlantic. *Deep-Sea Res.*, 38, S323–S343.

——, S. E. Zebiak, and K. Bryan, 1992: Climate variability and the Atlantic Ocean. *Eos, Trans. Amer. Geophys. Union*, 73, 161–165.

Gottschee, A., M. Latif, and T. P. Barnett, 1998: A decadal climate cycle in the North Atlantic Ocean as simulated by the ECHO coupled GCM. *J. Climate*, 11, 831–847.

Gu, D., and S. G. H. Philander, 1995: Secular changes of annual and interannual variability in the Tropics during the past century. *J. Climate*, 8, 864–876.

Hallinwell, G. R., Jr., 1995: Decadal and multi-decadal North Atlantic SST anomalies driven by standing and propagating basin scale atmospheric anomalies. *J. Climate*, 10, 2405–2411.

Hameed, S., K. R. Spreber, and A. Meinster, 1997: Teleconnections of the Southern Oscillation in the tropical Atlantic sector in the OSU coupled ocean–atmosphere GCM. *J. Climate*, 10, 2405–2411.

Hansen, D. V., and H. F. Bezdek, 1996: On the nature of decadal anomalies in North Atlantic sea surface temperature. *J. Geophys. Res.*, 101, 8749–8758.

Hastenrath, S., and L. Heller, 1977: Dynamics of climatic hazards in northeastern Brazil. *Quart. J. Roy. Meteor. Soc.*, 103, 77–92.

——, L. C. Castro, and P. Aceituno, 1987: The Southern Oscillation in the tropical Atlantic sector. *Contrib. Atmos. Phys.*, 60, 447–463.

Henin, C., and P. Hisard, 1987: The North Equatorial Counter Current observed during the "Programme Français Océan et Climat dans l'Atlantique Equatorial," July 1982 to August 1984. *J. Geophys. Res.*, 92, 3751–375.

Hisard, P., 1980: Observation de réponse de type El Niño dans l'Atlantique tropical oriental Golfe de Guinée. *Oceanol. Acta*, 3, 69–78.

——, and C. Henin, 1987: Response of the equatorial Atlantic Ocean to the 1983–4 wind from the FOCAL cruise data set. *J. Geophys. Res.*, 92, 3759–3768.

Hogg, N. G., R. Pickart, R. M. Hendry, and W. Smethie, 1986: The northern recirculation gyre of the Gulf Stream. *Deep-Sea Res.*, 33, 1139–1165.

Houghton, R. W., 1996: Subsurface quasi-decadal fluctuations in the North Atlantic. *J. Climate*, 9, 1363–1373.

——, and Y. M. Tourre, 1992: Characteristics of low frequency sea surface temperature fluctuations in the tropical Atlantic. *J. Climate*, 5, 765–771.

Hurrell, J. W., 1995: Decadal trends in the North Atlantic oscillation regional temperatures and precipitation. *Science*, 269, 676–679.

——, and H. van Loon, 1996: Decadal variations in climate associated with the North Atlantic oscillation. *Climate Change*, 36, 301–326.

Jin, F.-F, 1996: Tropical ocean–atmosphere interaction, the Pacific cold tongue, and the El Niño Southern Oscillation. *Science*, 274, 76–78.

Kaplan, A., M. A. Cane, Y. Kushnir, A. C. Clement, M. B. Blumenthal, and B. Rajagopalan, 1997: Analyses of global sea surface temperature 1856–1991. *J. Geophys. Res.*, 102, 27 835–27 860.

——, ——, and ——, 1998: Reduced space optimal interpolation of historical sea level pressure: 1854–1992. *J. Geophys. Res.*, 103, 18 567–18 589.

Kawamura, R., 1994: A rotated EOF analysis of global sea surface temperature variability with interannual and interdecadal scales. *J. Phys. Oceanogr.*, 24, 707–715.

Kondo, M., H. Imasato, and A. Shibata, 1996: Analysis of the global relationship of biennial variation of sea surface temperature and air–sea heat flux using satellite data. *J. Oceanogr.*, 52, 717–746.

Kushnir, Y., 1994: Interdecadal variations in the North Atlantic sea surface temperature and associated atmospheric conditions. *J. Climate*, 7, 141–157.

——, 1996: Long-term climate variability in the north Atlantic and adjacent continents. *Proc. JCESS-CLIVAR Workshop on Decadal climate variability*. NASA-University of Maryland, Department of Meteorology, University of Maryland, College Park, MD, 27–31.

——, B. Rajagopalan, and Y. M. Tourre, 1998: Decadal climate variability in the Atlantic basin. Preprints, *Ninth Conf. on Air–Sea Interaction*, Phoenix, AZ, Amer. Meteor. Soc., 58–61.

Kutzbach, J. E. 1970: Large-scale features of monthly mean Northern Hemisphere anomaly maps of sea-level pressure. *Mon. Wea. Rev.*, 98, 708–716.

Lall, U., K. Bosworth, and A. Owosina, 1999: Local polynomial estimate of spatial surfaces. *Comput. Stat.*, in press.

Landsberg, H. E., J. M. Mitchell Jr., H. L. Crutcher, and F. T. Quinlan, 1963: Surface signs of the biennial atmospheric pulse. *Mon. Wea. Rev.*, 91, 549–556.

Lanzante, J. R., 1996: Lag relationships involving tropical sea surface temperature. *J. Climate*, 9, 2568–2578.

Latif, M., and T. P. Barnett, 1994: Causes of decadal variability over the North Pacific and North America. *Science*, 226, 634–637.

——, and ——, 1995: Interactions of the tropical oceans. *J. Climate*, 8, 952–964.

Lau, N.-C., and M. J. Nath, 1990: A general circulation model study of the atmospheric response to extra tropical SST anomalies observed in 1950–79. *J. Climate*, 3, 965–989.

——, and ——, 1996: The role of the "atmospheric bridge" in linking tropical Pacific ENSO to extra tropical SST anomalies. *J. Climate*, 9, 2036–2057.

Levitus, S., 1989: Interpentedal variability of temperature and salinity in the deep North Atlantic, 1970–1974 versus 1955–1959. *J. Geophys. Res.*, 94, 16 125–16 131.

——, and A. H. Oort, 1977: Global analysis of oceanographic data. *Bull. Amer. Meteor. Soc.*, 58, 1270–1284.

——, J. Antonov, and T. P. Boyer, 1994: Interannual variability of temperature at a depth of 125 meters in the north Atlantic Ocean. *Science*, 266, 96–99.

Lindzen, R. S., and S. Nigam, 1987: On the role of sea surface temperature gradients in forcing low level winds and convergence in the Tropics. *J. Atmos. Sci.*, 44, 2440–2458.

Lu, P., and J. P. McCreary, 1995: Influence of the ITCZ in the flow of thermocline water from the subtropical to the equatorial Pacific Ocean. *J. Phys. Oceanogr.*, 25, 3076–3088.

Mann, M. E., and J. Park, 1994: Global-scale modes of surface temperature variability on interannual to century time scales. *J. Geophys. Res.*, 99, 25 819–25 833.
——, and ——, 1996: Joint spatio-temporal modes of surface temperature and sea level pressure variability in the Northern Hemisphere during the last century. *J. Climate*, 9, 2137–2162.
——, and ——, 1999: Oscillatory spatio-temporal signal detection in climate studies: a multi-taper spectral domain approach. *Advances In Geophysics*, in press.
Mechoso, C. R., S. W. Lyons, and J. A. Spahr, 1990: The impact of sea surface temperature anomalies on the rainfall over Northeast Brazil. *J. Climate*, 3, 812–826.
Mehta, V. M., and T. Delworth, 1995: Decadal variability of the tropical Atlantic Ocean surface temperature in shipboard measurements and in global ocean–atmosphere model. *J. Climate*, 8, 172–190.
Melloc, G. L., C. R. Mechoso, and E. Keto, 1982: A diagnostic calculation of the general circulation of the Atlantic Ocean. *Deep-Sea Res.*, 29, 1171–1192.
Merle, J., 1980: Variabilité thermique et interannuelle de l'Ocean Atlantique equatorial Est. L'hypothese d'un "El Niño" Atlantique. *Oceanol. Acta*, 3, 209–220.
Molinari, R. L., D. Meyer, J. F. Festa, and H. F. Bezdek, 1997: Multiyear variability in the near surface temperature structure of the mid latitude western North Atlantic Ocean. *J. Geophys. Res.*, 102, 3267–3278.
Neelin, J. D., M. Latif, and F. F. Jin, 1994: Dynamics of coupled ocean–atmosphere models: The tropical problem. *Annu. Rev. Fluid Mech.*, 26, 617–659.
Nobre, C., 1985: CCCO Atlantic panel report. Rio de Janeiro, ICSU Publ. [Available from UNESCO, 1 rue Miollis, Paris 75007, France.]
Park, J., C. R. Lindberg, and F. L. Vernon III, 1987: Multitaper spectral analysis of high-frequency seismograms. *J. Geophys. Res.*, 92, 12 675–12 684.
Peterson, R. G., and W. B. White, 1998: Slow oceanic teleconnections linking the Antarctic Circumpolar Wave with the tropical El Niño–Southern Oscillation. *J. Geophys. Res.*, 103, 24 573–24 583.
Philander, S. G. H., 1986: Unusual conditions in the tropical Atlantic Ocean in 1984. *Nature*, 322, 236–238.
——, 1990: *El Niño, La Niña and the Southern Oscillation.* International Geophysics Series, Vol. 46, Academic Press, 293 pp.
——, and R. C. Pacanowski, 1981: The oceanic response to cross-equatorial winds (with application to coastal upwelling in low latitudes). *Tellus*, 33, 201–210.
Piotrowski, I. I., and S. Hameed, 1991: Simulation of the North Atlantic Oscillation in a general circulation model. *Geophys. Res. Lett.*, 18, 841–844.
Rajagopalan B., U. Lall, and M. A. Cane, 1997: Anomalous ENSO occurences—An alternate view. *J. Climate*, 10, 2351–2357.
——, Y. Kushnir, and Y. M. Tourre, 1998: Midlatitude and tropical Atlantic climate variability. *Geophys. Res. Lett.*, 25, 3967–3970.
Rasmusson, E. M., and P. A. Arkin, 1985: Interannual climate variability associated with the El Niño Southern Oscillation. *Proceedings JSC/CCCO International Liege Colloquium: Coupled Ocean–Atmosphere Models*, J. C. J. Nihoul, Ed., Elsevier Publishers, 697–723.
Reid, J. L., 1989: On the total geostrophic circulation of the south Atlantic Ocean: Flow patterns, tracers and transports. *Progress In Oceanography*, Vol. 23, Pergamon Press, 149–244.
Reverdin, G., and M. J. McPhaden, 1986: Near surface current and temperature variability observed in the equatorial Atlantic from drifting buoys. *J. Geophys. Res.*, 91, 6569–6581.
——, P. Delecluse, C. Levy, P. Andrich, A. Morliere, and J. M. Verstraete, 1991: The near surface tropical Atlantic during 1982–4—Results from a numerical simulation and a data analysis. *Progress In Oceanography*, Vol. 27, Pergamon Press, 273–340.
——, D. Cayan, and Y. Kushnir, 1997: Decadal variability of hydrography in the upper North Atlantic, 1948–1990. *J. Geophys. Res.*, 102, 8505–8531.
Rogers, J. C., 1984: The association between the North Atlantic Oscillation and the Southern Oscillation in the Northern Hemisphere. *Mon. Wea. Rev.*, 112, 1999–2015.
Servain, J., 1991: Simple climatic indices for the tropical Atlantic Ocean and some applications. *J. Geophys. Res.*, 96, 15 137–15 146.
Shannon, L. V., A. J. Boyd, G. B. Brundrit, and J. Taunton-Clark, 1986: On the existence of an El Niño type phenomenon in the Benguela system. *J. Mar. Res.*, 44, 495–520.
Spetbec, K. R., and S. Hameed, 1993: Phase locking of Northeast precipitation with sea surface temperatures. *Geophys. Res. Lett.*, 20, 113–116.
Stramma, L., 1991: Geostrophic transport of the South Equatorial Current in the Atlantic. *J. Mar. Res.*, 49, 281–294.
Sutton, R. T., and M. R. Allen, 1997: Decadal predictability in North Atlantic sea surface temperature and climate. *Nature*, 388, 563–567.
Thomson, D. J., 1982: Spectrum estimation and harmonic analysis. *IEEE Proc.*, 70, 1055–1096.
Tinsley, B. A., 1988: The solar cycle and QBO influence on the latitude of storm tracks in the North Atlantic. *Geophys. Res. Lett.*, 15, 409–412.
Tourre, Y. M., and W. B. White, 1995: ENSO signals in global upper-ocean temperature. *J. Phys. Oceanogr.*, 25, 1317–1332.
——, M. Decqué, and J. F. Royer, 1985: Atmospheric response of a general circulation model forced by a sea surface temperature distribution analogous to the winter 1982–1983 El Niño. *Coupled Ocean–Atmosphere Models*, J. C. J. Nihoul, Ed., Elsevier Publishers, 479–490.
——, Y. Kushnir, and W. B. White, 1999: Evolution of interdecadal variability in sea level pressure, sea surface temperature and upper ocean temperature over the Pacific Ocean. *J. Phys. Oceanogr.*, 29, 1528–1541.
Trenberth, K. E., and W. T. K. Shin, 1984: Quasi-biennial fluctuations in sea level pressures over the Northern Hemisphere. *Mon. Wea. Rev.*, 112, 761–777.
van Loon, H., and J. C. Rogers, 1978: The seesaw in winter temperatures between Greenland and northern Europe. Part I: General description. *Mon. Wea. Rev.*, 106, 296–310.
Venegas, S. A., L. A. Mysak, and D. N. Straub, 1997: Atmosphere–ocean coupled variability in the South Atlantic. *J. Climate*, 10, 2904–2920.
Wagner, A. J., 1971: Long-period variations in seasonal sea-level pressure over the Northern Hemisphere. *Mon. Wea. Rev.*, 99, 49–66.
Wagner, R. G., 1996: Mechanisms controlling variability of the inter-hemispheric sea surface temperature gradient in the tropical Atlantic. *J. Climate*, 9, 2010–2019.
Wainer, I., and J. Soares, 1997: North-northeast Brazil rainfall and its decadal scale relationship to wind stress and sea surface temperature. *Geophys. Res. Lett.*, 24, 277–280.
Wallace, J. M., and D. S. Gutzler, 1981: Teleconnections in the geopotential height field during the Northern Hemisphere winter. *Mon. Wea. Rev.*, 109, 784–812.
White, W. B., and R. G. Peterson, 1996: An Antarctic circumpolar wave in surface pressure, wind, temperature and sea-ice extent. *Nature*, 380, 699–702.
Wohlleben, T. M. H., and A. J. Weaver, 1995: Interdecadal climate variability in the subpolar North Atlantic. *Climate Dyn.*, 11, 459–467.
Wolter, K., 1989: Modes of tropical circulation, Southern Oscillation, and Sahel rainfall anomalies. *J. Climate*, 2, 149–172.
Zebiak, S., 1993: Air-sea interaction in the equatorial Atlantic region. *J. Climate*, 6, 1567–1586.
Zhang, Y., J. M. Wallace, and D. Battisti, 1997: ENSO-like interdecadal variability: 1900–93. *J. Climate*, 10, 1004–1020.